PERGAMON

International Journal of Heat and Mass Transfer 43 (2000) 3661–3671

International Journal of HEAT and MASS TRANSFER

www.elsevier.com/locate/ijhmt

Closed-form analytical solutions for radially rotating miniature high-temperature heat pipes including non-condensable gas effects

Jian Ling, Yiding Cao*

Department of Mechanical Engineering, Florida International University, University Park, Miami, FL 33199, USA

Received 17 June 1999; received in revised form 22 October 1999

Abstract

The radially rotating miniature high-temperature heat pipe is a wickless heat pipe, which has a simple structure and low manufacturing cost, and can withstand strong vibrations in a high-temperature environment. In this paper, the radially rotating miniature high-temperature heat pipe having a diameter in the range of 1.5–2 mm is analyzed by employing appropriate flow and heat transfer models as well as experimental investigation. The diffuse effects of non-condensable gases on temperature distribution along the heat pipe length are investigated. Closed-form analytical solutions for the temperature distribution along the heat pipe length are obtained and extensive experimental tests are undertaken. These closed-form analytical solutions are in good agreement with the experimental data. The theoretical and experimental studies prove that the radially rotating miniature high-temperature heat pipe with sodium as the working fluid has a very large heat transfer capability and a high effective thermal conductance that is 60–100 times higher than the thermal conductivity of copper. Although the diffuse effects of the non-condensable gases would increase temperature drop along the heat pipe length, the heat pipes can still work effectively and reliably. As a result, the combination of the traditional air-cooling technology with radially rotating miniature heat pipes is a feasible and effective cooling means for the rotor blades of a high-temperature gas turbine.

1. Introduction

Effective cooling of gas turbine blades and disks is crucial to protecting metal surfaces from hostile thermal environments. The turbine blade and disk cooling incorporating the radially rotating miniature high-temperature heat pipe is a new approach towards this goal. The radially rotating miniature high-temperature heat pipe, which rotates about the axis of revolution, is a wickless heat pipe that is comprised of an air-evacuated hollow container and an amount of working fluid sealed within the container, as shown in Fig. 1. The centrifugal force generated by the rotating motion of the heat pipe is utilized for the return of the liquid condensate from the condenser to the evaporator [1–4]. Analytical solutions for the liquid film distributions in the condenser section and temperature drops along the heat pipe length without the diffuse effects of non-condensable gases have been obtained [5–9]. At a moderate high rotating speed, the liquid film is very thin and its effect on the temperature distribution along the heat pipe is negligible [10] [11]. The temperature distribution along the heat pipe length is largely determined

* Corresponding author.

0017-9310/00/$ - see front matter
PII: S0017-9310(99)00339-7

Nomenclature

A	cross-sectional area (m^2)
a	constant
Bo	Bond number
c	constant
d	heat pipe diameter (m)
F_v	frictional coefficient
f	skin-friction coefficient
g	gravitational acceleration (m/s^2)
h_c	heat transfer coefficient (W/m^2 °C)
h_{fg}	latent heat of evaporation (J/kg)
k	thermal conductivity (W/m °C)
L	heat pipe length (m)
m	coefficient (1/m)
$\dot{m}$	mass flow rate (kg/s)
m_v	Mach number
p	pressure (N/m^2)
Q	heat transfer rate (W)
q''	heat flux (W/m^2)
Re	Reynolds number
r	heat pipe radius (m)
T	temperature (°C)
w	axial velocity (m/s)
W	flow rate of cooling air (m^3/s)
z	axial location of the heat pipe (m)
$\bar{Z}$	revolving radius of the heat pipe (m)
ϕ	tilt angle between the heat pipe centerline and engine radial line (°)
θ	rotating angle of the heat pipe (°)
ρ	density (kg/m^3)
μ	dynamic viscosity (kg/m s)
τ	shear stress (N/m^2)
ω	angular velocity (rad/s)

Subscripts

a	adiabatic section
c	condenser
e	evaporator
eff	effective
i	inner
o	outer
p	heat pipe wall
v	vapor phase
z	axial location of the heat pipe

by the temperature drop associated with the vapor flow. On the other hand, because of the wickless structure and a very small volume, it is unavoidable that a small amount of non-condensable gases is trapped in the heat pipe during the process of heat pipe charging and sealing. In some other cases, it would be preferable to charge an amount of non-condensable gas in the heat pipe to prevent the condenser end, which is attached to other components, from becoming too hot. The pure vapor flow in a radially rotating heat pipe without the effect of a non-condensable gas has been studied extensively in the past. These studies have been included in the aforementioned references such as those by Cao et al. [10] and Ling et al. [11]. The existence of a non-condensable gas in the heat pipe will significantly affect the heat pipe performance. However, the radially rotating miniature high-temperature heat pipe including non-condensable gases has not been studied earlier, and will be the major focus of this paper.

2. Temperature distribution along the heat pipe length without the effects of non-condensable gases

Consider a one-dimensional laminar and incompressible vapor flow along the heat pipe length under the steady-state operating condition, as shown in Fig. 2, where $f_c = \rho_v \omega^2 \bar{Z} \pi R_v^2 \sin\phi \, dz$ is the vapor centrifugal force, and $f_g = \rho_v g \pi R_v^2 \sin\phi \cos\theta \, dz$ is the vapor gravitational force. Based on the force and thermal balances over the control volume, the following relations for the vapor pressure gradient and shear stress are derived:

$$\frac{dp_v}{dz} = \frac{2}{R_v \sin\phi}\tau_{v,R} + \rho_l\left(\omega^2\bar{Z} - g\cos\theta\right) - \frac{d}{dz}(\dot{m}_v\bar{w}_v)\frac{1}{\sin\phi} \tag{1}$$

$$\tau_{v,R_v} = (fRe)_v \frac{\mu_v \bar{q}_c'' z}{2R_v^2 \rho_v h_{fg}} \tag{2}$$

$$\frac{d(m_v\bar{w}_v)}{dz} = 2\pi R_v^2 \rho_v \bar{w}_v \frac{d\bar{w}_v}{dz} = \frac{8\pi \bar{q}_c''^{\,2} z}{\rho_v h_{fg}^2} \tag{3}$$

where $R_v = R - \delta$ is the vapor space radius in the heat pipe, $\dot{m}_v$ is the vapor mass flow rate, $\bar{w}_v$ is the average vapor velocity over the heat pipe cross-sectional area, $\bar{Z} = z_0 + z\sin\phi$ is the revolving radius of the control volume, and f is the laminar vapor skin-friction coefficient. Plugging Eqs. (2) and (3) into Eq. (1) gives

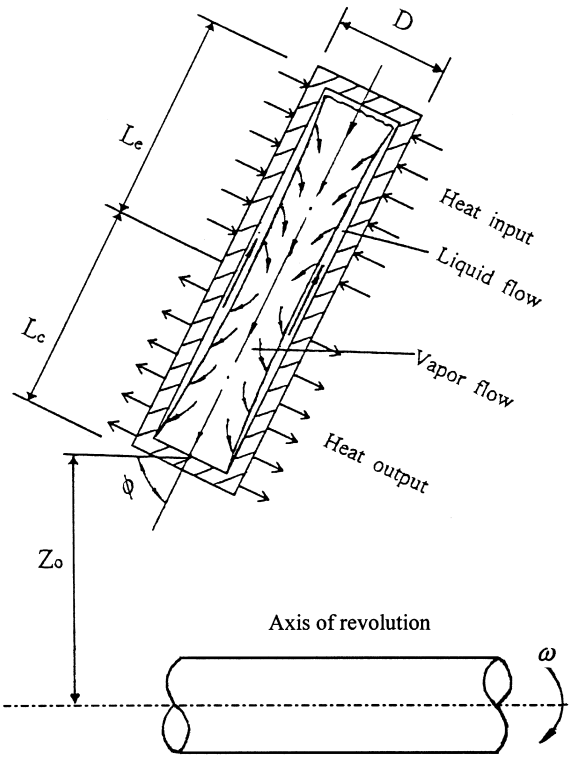

Fig. 1. Schematic of a radially rotating heat pipe with a tilt angle.

$$\frac{dp_v}{dz} = (fRe)_v \frac{\mu_l \bar{q}_c'' z}{R_v^3 \rho_v h_{fg} \sin\phi} + \rho_l\left(\omega^2 \bar{Z} - g\cos\theta\right) - \frac{8\pi \bar{q}_c''^{\,2} z}{\rho_v h_{fg}^2 \sin\phi} \tag{4}$$

In general, the above equations are valid when the following two conditions in terms of the vapor Reynolds number and Mach number are satisfied:

$$Re_v = \frac{2R_v Q}{A_v \mu_v h_{fg}} \le 2300 \tag{5}$$

$$M_v = \frac{Q}{A_v \rho_v h_{fg} \sqrt{\gamma_v R_g T_v}} \le 0.3 \tag{6}$$

where A_v is the cross-sectional area of the vapor space, γ_v is the vapor specific heat ratio, and R_g is the vapor gas constant [4]. These two conditions can usually be satisfied for high-temperature heat pipes having a small diameter and operating at a steady state.

The last term on the right-hand side of Eq. (4) is usually negligible compared to the other terms. Eq. (4) thus becomes:

$$\frac{dp_v}{dz} = (fRe)_v \frac{\mu_l \bar{q}_c'' z}{R_v^3 \rho_v h_{fg} \sin\phi} + \rho_l\left(\omega^2 \bar{Z} - g\cos\theta\right) \tag{7}$$

In addition, for the current practical applications, the adiabatic length, L_a, is zero. Therefore, the heat pipe is divided only into the evaporator and condenser sections. Integrating Eq. (7) from 0 to z based on the mass and energy balances under the conditions of steady state and $L_a = 0$ yields:

$$\Delta p_{v,z} = \frac{F_v Q_c z^2}{2L_c \sin\phi} + \rho_v\left[\omega^2\left(z_0 + \frac{1}{2} z \sin\phi\right) z - g\cos\theta\right]$$

$$\text{at} \quad 0 \le z \le L_c \tag{8}$$

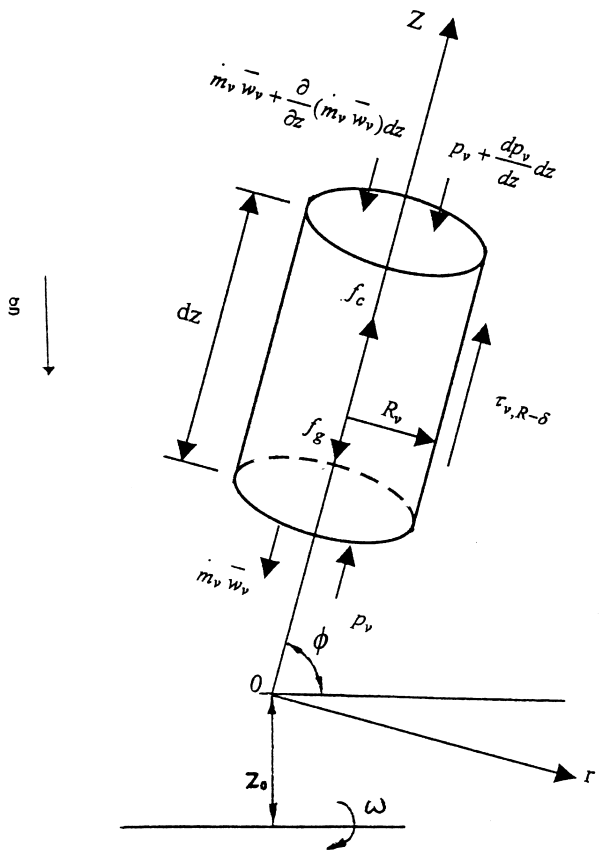

Fig. 2. Schematic of a thermal balance for the vapor flow in the condenser section.

$$\Delta p_{\mathrm{v},z} = \frac{F_{\mathrm{v}} Q_{\mathrm{c}}}{2\sin\phi}\left[L - \frac{(L-z)^2}{L-L_{\mathrm{c}}}\right] + \rho_{\mathrm{v}}\left[\omega^2\left(z_0 + \frac{1}{2}z\sin\phi\right)z - g\cos\theta\right] \quad \text{at} \quad L_{\mathrm{c}} \le z \le L \tag{9}$$

The vapor gravitational force can be neglected compared to the centrifugal force in Eqs. (8) and (9). Assuming the vapor is saturated and employing the Clapeyron Equation, the vapor temperature drop is obtained from the pressure drop:

$$\Delta T_{\mathrm{v},z} = \begin{cases} \dfrac{T_{\mathrm{v}} F_{\mathrm{v}} Q_{\mathrm{c}}}{2h_{fg}\rho_{\mathrm{v}} L_{\mathrm{c}}\sin\phi} z^2 + \dfrac{T_{\mathrm{v}}}{h_{fg}}\left[\omega^2\left(z_0 + \dfrac{1}{2}z\sin\phi\right)z\right] & (0 \le z \le L_{\mathrm{c}}) \\ \dfrac{T_{\mathrm{v}} F_{\mathrm{v}} Q_{\mathrm{c}}}{2h_{fg}\rho_{\mathrm{v}}\sin\phi}\left[L - \dfrac{(L-z)^2}{L-L_{\mathrm{c}}}\right] + \dfrac{T_{\mathrm{v}}}{h_{fg}}\left[\omega^2\left(z_0 + \dfrac{1}{2}z\sin\phi\right)z\right] & (L_{\mathrm{c}} \le z \le L) \end{cases} \tag{10}$$

Since

$$\Delta T_{\mathrm{v},z} = T_{\mathrm{v},z} - T_{\mathrm{v},z_0} \tag{11}$$

$$T_{\mathrm{v},z_0} = T_{\mathrm{v},L} - \Delta T_{\mathrm{v},L} = T_{\mathrm{v},L} - \left[\frac{T_{\mathrm{v}} F_{\mathrm{v}} Q_{\mathrm{c}} L_{\mathrm{eff}}}{h_{fg}\rho_{\mathrm{v}}\sin\phi} + \frac{T_{\mathrm{v}}}{h_{fg}}\omega^2\left(z_0 + \frac{1}{2}L\sin\phi\right)L\right] \tag{12}$$

Substituting Eqs. (10) and (12) into Eq. (11) and rearranging it, yields

$$T_{\mathrm{v},z} = T_{\mathrm{v},z_0} + \Delta T_{\mathrm{v},z} = T_{\mathrm{v},L} - \begin{cases} \left\{\dfrac{T_{\mathrm{v}} F_{\mathrm{v}} Q_{\mathrm{c}}}{h_{fg}\rho_{\mathrm{v}}\sin\phi}\left(L_{\mathrm{eff}} - \dfrac{z^2}{2L_{\mathrm{c}}}\right) + \dfrac{T_{\mathrm{v}}\sin\phi}{h_{fg}}\omega^2\left[\left(z_0 + \dfrac{1}{2}L\right)L - \left(z_0 + \dfrac{1}{2}z\right)z\right]\right\} & 0 \le z \le L_{\mathrm{c}} \\ \left\{\dfrac{T_{\mathrm{v}} F_{\mathrm{v}} Q_{\mathrm{c}}}{h_{fg}\rho_{\mathrm{v}}\sin\phi}\left[L_{\mathrm{eff}} - \dfrac{1}{2}\left(L - \dfrac{(L-z)^2}{L-L_{\mathrm{c}}}\right)\right] + \dfrac{T_{\mathrm{v}}\sin\phi}{h_{fg}}\omega^2\left[\left(z_0 + \dfrac{1}{2}L\right)L - \left(z_0 + \dfrac{1}{2}z\right)z\right]\right\} & L_{\mathrm{c}} \le z \le L \end{cases} \tag{13}$$

where T_{v,z_0} and $T_{\mathrm{v},L}$ are the temperatures at the condenser and evaporator ends, respectively.

Eq. (13) is a closed-form analytical solution for the temperature distribution along the heat pipe length. It should be pointed out that Eq. (13) only includes the effects of vapor friction and centrifugal force on the temperature distribution. If non-condensable gases exist in the heat pipe, the diffuse effects of the non-condensable gases on temperature distribution must be considered.

3. Diffuse effects of non-condensable gases and closed-form analytical solutions for the temperature distribution

The non-condensable gases in the heat pipe will be driven to the condenser end by the vapor flow from the evaporator, which prevents the vapor from filling the entire condenser section. Therefore, the temperature distribution along the condenser wall will no longer be uniform, and a large temperature gradient will appear in the condenser section as a result of the existence of the non-condensable gases. Marcus [12] first developed a numerical model based on one-dimensional diffusion of the vapor–gas system coupled with one-dimensional axial heat conduction in the wall for variable conductance heat pipes. Numerical results indicated that the axial heat conduction played a dominant role in the determination of the temperature distribution along the heat pipe wall.

For a radially rotating heat pipe, the vapor–gas interface between the vapor and non-condensable gases is assumed to be a flat front. Fig. 3 shows schematically a thermal balance for the heat pipe wall in the condenser section. A control volume with a cross-sectional area of $\pi(r_{\mathrm{o}}^2 - r_{\mathrm{i}}^2)$ and an infinitesimal length of dz is considered. Based on the conservation of energy, the following equation is obtained:

$$\pi\left(r_o^2 - r_{\mathrm{i}}^2\right)k_{\mathrm{p}}\frac{\mathrm{d}^2 T}{\mathrm{d}z^2} - 2\pi r_o h_{\mathrm{c}}\left(T_{\mathrm{p}} - T_{\mathrm{s}}\right) + Q' = 0 \tag{14}$$

Since the radial temperature drop in the heat pipe wall is much smaller than the axial temperature drop, the

radial temperature drop is neglected as a first approximation, i. e., $T_p = T$. Eq. (14) thus can be rearranged as:

$$\frac{d^2T}{dz^2} - m^2\left(T - T_s - \frac{Q'}{2\pi r_o h_c}\right) = 0 \tag{15}$$

where $m^2 = \dfrac{2r_o h_c}{k_p(r_o^2 - r_i^2)}$

h_c is the mean heat transfer coefficient, Q' is the heat output in the condenser section without non-condensable gases, T is the axial temperature which is a function of z, T_p and T_s are the outer surface temperature of the heat pipe and the surrounding temperature, respectively.

Assuming the distribution of Q' is uniform in the portion of the condenser section without non-condensable gases, and zero in the portion of the condenser section with non-condensable gases, then

$$Q' = 0 \quad \text{at} \quad 0 \le z \le L_{c,\,n} \tag{16}$$

$$Q' = \frac{Q_c}{L_c - L_{c,n}} \quad \text{at} \quad L_{c,n} \le z \le L_c \tag{17}$$

where Q_c is the total heat output in the condenser section; L_c is the length of the total condenser section, and $L_{c,\,n}$ is the length occupied by non-condensable gases in the condenser section.

At the inlet of the condenser section, the axial heat conduction is negligible. As a result,

$$Q_c \cong 2\pi r_o(L_c - L_{c,\,n})h_c(T_{L_c} - T_s) \tag{18}$$

where T_{L_c} is the temperature at the condenser inlet. Substituting Eq. (18) into (17) and recasting it yield:

$$\frac{Q'}{2\pi r_o h_c} = T_{L_c} - T_s \quad \text{at} \quad L_{c,\,n} \le z \le L_c \tag{19}$$

Plugging Eqs. (19) and (16) into Eq. (15) gives

$$\frac{d^2T}{dz^2} - m^2(T - T_s) = 0 \quad \text{at} \quad 0 \le z \le L_{c,\,n} \tag{20}$$

$$\frac{d^2T}{dz^2} - m^2(T - T_{L_c}) = 0 \quad \text{at} \quad L_{c,\,n} \le z \le L_c \tag{21}$$

For a radially rotating miniature heat pipe, the boundary conditions are:

$$\frac{dT}{dz} = 0 \quad \text{at} \quad z = -\infty \tag{22}$$

$$T = T_{L_c} \quad \text{at} \quad z = L_c \tag{23}$$

According to the overall energy balance in the condenser section, the following relation is obtained:

$$\int_0^{L_c} 2\pi r_o h_c(T - T_c)\,dz = Q_c \tag{24}$$

The solutions for Eqs. (20) and (21) after incorporating the boundary conditions are as follows:

$$T = a\exp(mz) + T_s \quad \text{at} \quad 0 \le z \le L_{c,\,n} \tag{25}$$

$$T = c\{\exp(mz) - \exp[m(2L_c - z)]\} + T_{L_c} \quad \text{at} \quad L_{c,\,n} \le z \le L_c \tag{26}$$

Due to the continuity of the axial temperature distribution along the heat pipe length, the temperature represented by Eqs. (25) and (26) must be equal at $z = L_{c,\,n}$. By employing this continuity condition in addition to the over energy balance condition represented

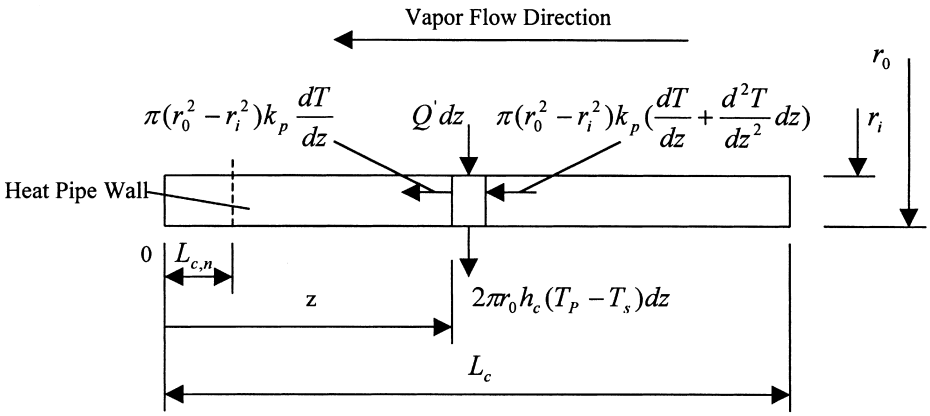

Fig. 3. Schematic of the diffuse effects of the non-condensable gases in the condenser section.

by Eq. (24), the constants c and a in Eqs. (25) and (26) are determined:

$$c = \frac{a\exp(mL_{c,n}) - (T_{L_c} - T_s)}{\exp(mL_{c,n}) - \exp[m(2L_c - L_{c,n})]} \tag{27}$$

$$a = \frac{(T_{L_c} - T_s)\{2\exp(mL_c) - \exp(mL_{c,n}) - \exp[m(2L_c - L_{c,n})]\}}{2\exp[m(L_c + L_{c,n})] + \exp[m(2L_c - L_{c,n})] - 2\exp(2mL_c) - \exp(mL_{c,n})} \tag{28}$$

Substituting the relations for coefficients a and c represented by Eqs. (27) and (28) into Eqs. (25) and (26) gives the temperature distribution including the diffuse effects of non-condensable gases along the condenser section.

For $L_{c,n} = 0$, it means that no non-condensable gases exist in the condenser section. Substituting $L_{c,n} = 0$ into Eqs. (27) and (28) yields:

$$a = T_{L_c} - T_s \quad \text{and} \quad c = 0$$

Plugging $a = T_{L_c} - T_s$ and $c = 0$ into Eqs. (25) and (26), one obtains:

$$T = T_{L_c} \quad 0 \le z \le L$$

The above relation means that the temperature distribution along the condenser section is uniform under the condition that no temperature drops are caused by the friction and the centrifugal force. It should be pointed out that since the radial temperature drop in the heat pipe wall is much smaller than the axial one and is neglected in the governing Eq. (15), the temperature in the heat pipe wall can be used to represent the vapor temperature in this region approximately.

Substituting $z = 0$ into Eq. (25), the temperature at the condenser end including the diffuse effects of non-condensable gases is obtained:

$$T'_{z_0} = T_s + a \quad \text{at} \quad z = 0 \tag{29}$$

Therefore, the temperature drops along the condenser section including the diffuse effects of non-condensable gases are as follows:

$$\Delta T_{n,z} = T - T'_{z_0} = \begin{cases} a[\exp(mz) - 1] & 0 \le z \le L_{c,n} \\ T_{L_c} - \{T_s + a + c[\exp(m(2L_c - z)) - \exp(mz)]\} & L_{c,n} \le z \le L_c \end{cases} \tag{30}$$

Usually, the amount of non-condensable gases in the condenser section is so small that their diffuse effects cannot reach the evaporator section. Accordingly, the temperature distribution in the evaporator section is not affected by the diffuse of non-condensable gases, and Eq. (13) is still suitable for the temperature distribution in the evaporator section. However, the temperature distribution along the condenser section will be affected strongly by the diffusion effects of non-condensable gases. At the same time, the vapor temperature drop, $\Delta T_{v,z}$, caused by the friction and centrifugal force, must be included in the temperature drop in the condenser section. If the temperature drop caused by the diffuse effects of non-condensable gases is superposed onto the temperature drop produced by the vapor friction and centrifugal force, the following relations are obtained:

$$\Delta T_z = \Delta T_{v,z} + \Delta T_{n,z} \tag{31a}$$

$$\Delta T_{n,L_c} = T_{L_c} - T'_{z_0} = T_{L_c} - T_s - a \tag{31b}$$

$$T_{z_0} = T_{v,L} - \Delta T_v - \Delta T_{n,L_c} \tag{31c}$$

$$\Delta T_z = T_{v,z} - T_{z_0} \tag{31d}$$

Therefore,

$$T_{v,z} = T'_{z_0} - \Delta T_v + \Delta T_{v,z} + \Delta T_{n,z} \tag{32}$$

It should be pointed out that the temperature drop caused by the vapor friction and centrifugal force must be dropped from Eq. (32) in the region of $0 \le z \le L_{c,n}$ since the vapor does not exist in this region. After the vapor temperature drops caused by vapor friction, centrifugal force, and diffuse effects of non-condensable gases are all considered, the vapor temperature distributions along the heat pipe length are as follows:

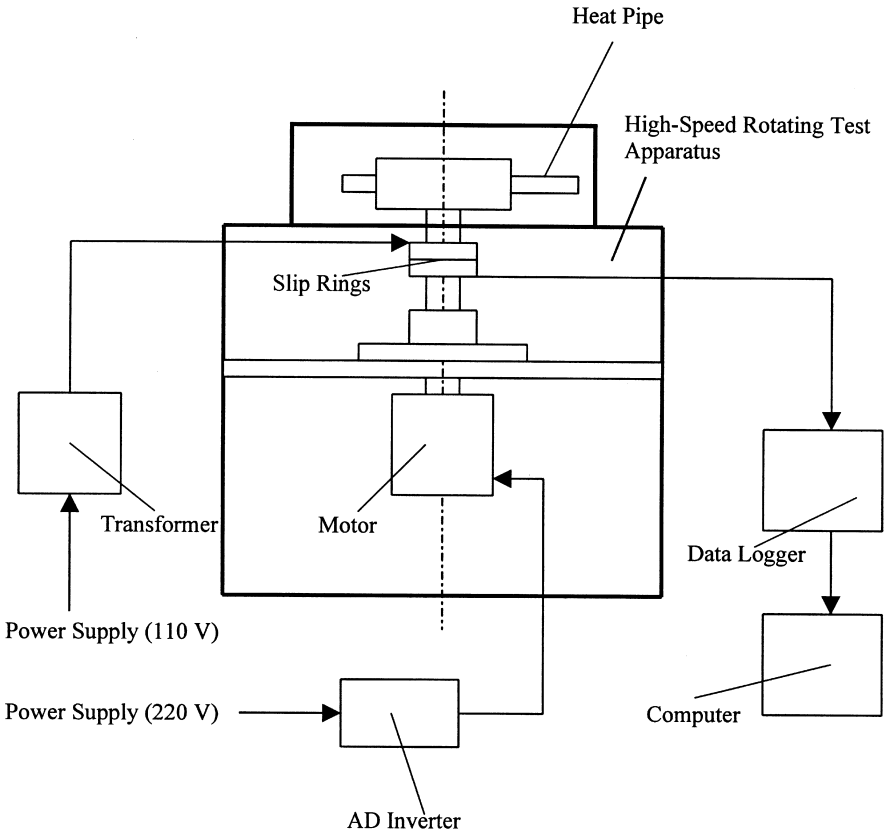

Fig. 4. Schematic of a high-speed rotating test apparatus and data acquisition system.

Evaporator section

$$T_{v,z} = T_{v,L} - \frac{T_v F_v Q_c}{h_{fg}\rho_v \sin\phi}\left\{L_{eff} - \left[L - \frac{(L-z)^2}{L-L_c}\right]\right\} - \frac{T_v\omega^2 \sin\phi}{h_{fg}}\left[z_0 + \tfrac{1}{2}L\right)L - \left(z_0 + \tfrac{1}{2}z\right)z] \qquad L_c \le z \le L \tag{33}$$

Condenser section

$$T_{v,z} = T_{v,L} - T_{L_c} + T_s + a - \Delta T_v + \Delta T_{v,z} + \Delta T_{n,z} = \begin{cases} \Delta T_{v,z} - \Delta T_v + T_{v,L} - c\left[\exp(m(2L_c - z)) - \exp(mz)\right] & L_{c,n} \le z \le L_c \\ T_{v,L} - T_{L_c} + T_s + a - \Delta T_v + a\left[\exp(mz) - 1\right] & 0 \le z \le L_{c,n} \end{cases} \tag{34}$$

where $m = \left[\dfrac{2r_o h_c}{k_p\left(r_o^2 - r_i^2\right)}\right]^{1/2}$

Eqs. (33) and (34) give a complete closed-form analytical solution for the temperature distribution along the radially rotating miniature heat pipe including the diffuse effects of non-condensable gases. $\Delta T_{v,z}$ in Eq. (34) is the vapor temperature drop caused by the friction and centrifugal forces along the direction z, which is given by Eq. (10). With a low and moderate rotating speed, $\Delta T_{v,z}$ is very small and negligible. ΔT_v in Eq. (34) is the total vapor temperature drop along the heat pipe length without the diffuse effects of non-conden-

Table 1
Comparisons of the temperature distributions and heat inputs between the heat pipe and heat pipe container with the same geometry

Dimensionless heat pipe length z/L	Temp. distribution for the heat pipe ($d_i = 2$ mm) (°C)	Temp. distribution for the heat pipe container ($d_i = 2$ mm) (°C)	Temp. distribution for the heat pipe ($d_i = 1.5$ mm) (°C)	Temp. distribution for the heat pipe container ($d_i = 1.5$ mm) (°C)
0.000	830.0	814.2	786.0	801.5
0.500	821.8	382.1	776.4	413.5
0.750	804.4	79.5	766.2	91.8
0.875	742.4	42.0	698.4	48.2
1.000	390.0	37.9	354.3	35.3

sable gases, which can be calculated by Eq. (10). For the heat pipe with fins on the outer surface of the condenser section, r_o may be replaced by the effective radius of the outer surface. T_v is the operating temperature of the heat pipe. In general, T_v can be replaced by $T_{v,L}$ as the designed operating temperature of the heat pipe.

4. High-speed rotating test apparatus and experimental study

To prove the foregoing analytical results, a high-speed rotating test apparatus and data acquisition system are constructed for the experimental study of radially rotating miniature high-temperature heat pipes, as shown in Fig. 4. The adjustable revolution range for the rotating test apparatus is 0–3600 rpm, which is controlled by an AC inverter. The maximum working temperature of the miniature heat pipe is 900°C. The electrical power is supplied to the heater through a two-channel slip ring, and the power is adjusted by a transformer from 0 to 120 V. The temperature distributions along the heat pipe are measured by five thermocouples. The temperature signals are fed to a data acquisition system through a 5-channel thermocouple slip ring. All experimental data, such as the heat input and temperature distributions along the heat pipe length, are scanned and recorded by the data acquisition system (HP 34970A, Data Acquisition/Switch Unit), and subsequently saved and displayed in a computer.

Two radially rotating miniature high-temperature heat pipes, which are made of stainless steel (Type 304W) and have a length of 80 mm, were tested on the high-speed rotating test apparatus. The two heat pipes have inner diameters of 1.5 mm and 2 mm, respectively. To facilitate the sodium charge for the heat pipes, a reservoir of 4 mm in diameter and 5 mm in length was attached to the tops of the evaporator sections. The sodium charge for the heat pipe having an inner diameter of 1.5 mm was approximately 0.06 g, and that for the heat pipe having an inner diameter of 2 mm was approximately 0.08 g. The two radially rotating miniature high-temperature heat pipes have the same outer diameter, 6 mm, and the same evapor-

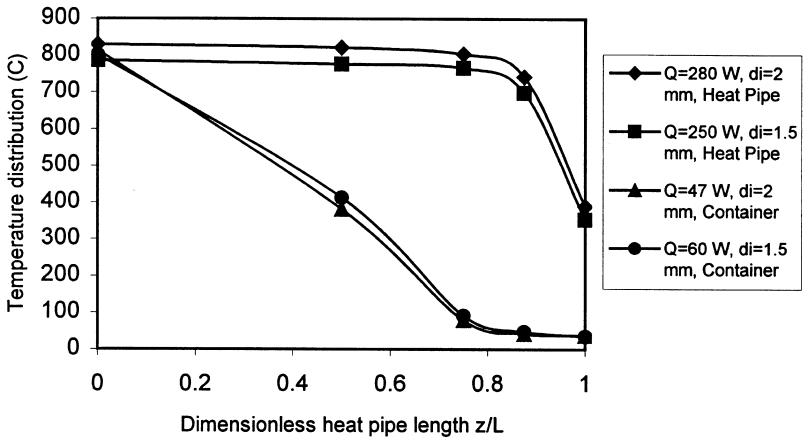

Fig. 5. Comparisons of temperature distributions and heat inputs between the heat pipe and heat pipe container ($\omega^2 \bar{Z}_a/g = 470$, and $W = 6.7 \times 10^{-3}$ m^3/s)

ator and condenser lengths of 40 mm, respectively. The heater was mounted on the evaporator sections firmly, and the insulation material of about 16 mm in thickness was clamped between the heater and a heater cap to ensure that the heat from the heater could be transferred into the evaporator section. For more detailed information regarding the experimental test, readers are referred to Ling and Cao [13].

5. Comparison of the analytical and the experimental results

To illustrate the effectiveness of the heat pipe, Table 1 and Fig. 5 show a comparison of the temperature distributions along the heat pipes and those along the heat pipe containers (the heat pipe shell without charging any fluid), with the same flow rate of cooling air, dimensionless centrifugal force, and geometrical dimensions. In the experiments, the tilt angle, ϕ, of the heat pipe was fixed at 90°. It can be seen from Table 1 and Fig. 5 that the heat transfer capacity of the heat pipe container is very low, which is 47 W for the heat pipe container with an inner diameter of 2 mm, and 60 W for that of 1.5 mm. The temperature distributions along most of the container length are approximately linear, and the temperature in the portion near the condenser end is close to the temperature of the cooling air. For the heat pipes, however, much more heat can be transferred; up to 280 W for the heat pipe with an inner diameter of 2 mm, and 250 W for that of 1.5 mm. If the thermal conductivity of copper is taken as

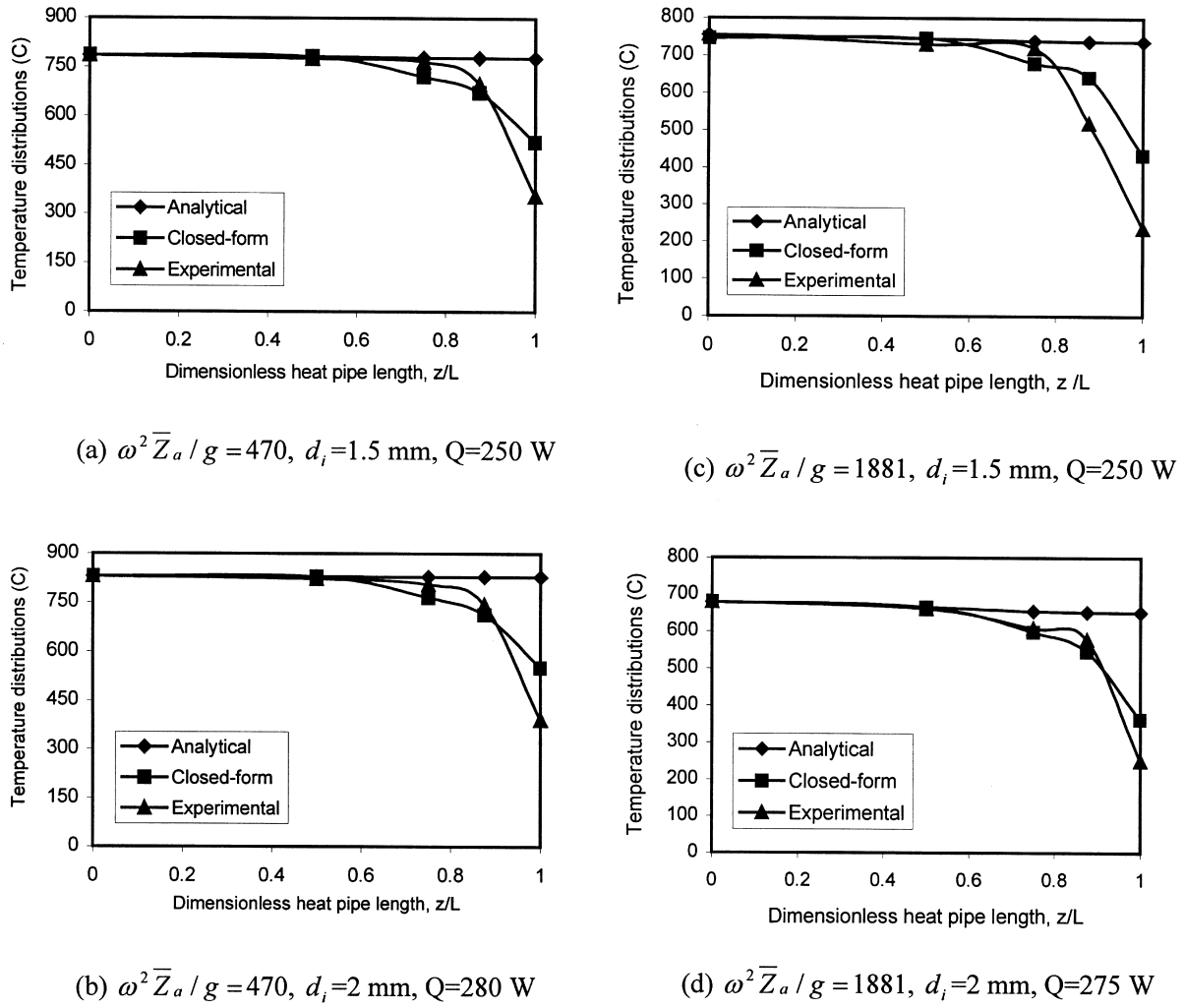

Fig. 6. Comparisons of analytical solutions, closed-form analytical solutions, and experimental results for the temperature distributions along the dimensionless heat pipe length ($L_{c,n} = 4$ mm).

Table 2
Comparisons of analytical solutions, closed-form analytical solutions and experimental results for the temperature distributions along dimensionless heat pipe length ($L_{c,n} = 4$) mm

Dimensionless heat pipe length z/L	Analytical solution without non-condensable gas (°C)	Closed-form solution with non-condensable gas (°C)	Experimental results (°C)
(a) $\omega^2\bar{Z}_a/g = 470$, $d_i = 1.5$ mm, $Q = 250$ W, $h_c = 226$ W/m^2 °C			
0.000	786.0	786.0	786.0
0.500	782.1	782.1	776.4
0.750	779.1	721.4	766.2
0.875	778.5	672.2	698.4
1.000	778.2	521.8	354.6
(b) $\omega^2\bar{Z}_a/g = 470$, $d_i = 2$ mm, $Q = 280$ W, $h_c = 297$ W/m^2 °C			
0.000	830.0	830.0	830.0
0.500	828.6	828.6	821.8
0.750	827.6	764.3	804.4
0.875	827.3	711.9	742.4
1.000	827.2	551.4	390.0
(c) $\omega^2\bar{Z}_a/g = 1881$, $d_i = 1.5$ mm, $Q = 250$ W, $h_c = 336$ W/m^2 °C			
0.000	754.5	754.5	754.5
0.500	745.5	745.5	730.0
0.750	739.5	680.3	720.0
0.875	737.8	642.2	520.0
1.000	737.2	433.8	235.7
(d) $\omega^2\bar{Z}_a/g = 1881$, $d_i = 2$ mm, $Q = 280$ W, $h_c = 392$ W/m^2 °C			
0.000	680.0	680.0	680.0
0.500	665.3	665.3	661.2
0.750	654.4	598.3	608.0
0.875	651.6	545.0	577.5
1.000	650.7	362.2	248.9

386 W/m °C, the effective heat conductance of the heat pipes is 60–100 times higher than the copper thermal conductivity, and 1100–1700 times higher than the thermal conductivity of the stainless steel used as the container of the heat pipe. These comparisons from Table 1 and Fig. 5 prove that radially rotating miniature high-temperature heat pipes can work very effectively and reliably. Their heat transfer characteristics are much better than that of any metal available.

Temperature distributions along the evaporator section and most of the condenser section are nearly uniform. It indicates that the heat pipe works perfectly in these sections. However a large temperature gradient is exhibited near the end cap of the condenser. This is because the condenser end is mounted onto the outer cylinder of the high-speed rotating test apparatus with a screw thread. As a result, an extra heat sink is formed at the condenser end, and some heat at the condenser end is transferred into the heat sink in the experiment, which results in a lower temperature near the condenser end.

The analytical solution based on Eq. (13) predicts the temperature distributions along the heat pipe length without the diffuse effects of non-condensable gases. Eqs. (33) and (34) give the analytical solutions of temperature distributions along the heat pipe length with the diffuse effects of non-condensable gases. These two analytical solutions for the temperature distributions are compared with the experimental results under the same operating conditions in Fig. 6a–d. In Eq. (13), the temperature distributions along the heat pipe length are caused only by the friction and the centrifugal forces of the vapor flow. Therefore, the temperature drops along the dimensionless heat pipe length are very small, and the temperature distributions are nearly straight lines, as shown in Fig. 6. The experimental data used in the comparison include the diffuse effects of non-condensable gases under the same operating conditions and geometrical dimensions. It can be seen that large discrepancies between the analytical solutions from Eq. (13) and the experimental results are present in the condenser sections, especially close to the condenser ends.

Eqs. (33) and (34) give the temperature distributions along the dimensionless heat pipe length with a flat front of vapor-gas interface when a portion of the condenser length, $L_{c,n} = 4$ mm, is occupied by non-condensable gases. Comparing the closed-form analytical solutions with the experimental data in Fig. 6, it is evident that the closed-form analytical solutions from

Eqs. (33) and (34) are more realistic than the analytical solutions from Eq. (13) and are closer to the experimental results. These comparisons are also presented in terms of tabulated form in Table 2. Based on the comparisons presented in both Table 2 and Fig. 6, it can be concluded that the closed-form analytical solutions from Eqs. (33) and (34) agree well with the experimental results in the entire evaporator section and most of the condenser section. Due to the existence of the heat sink at the condenser end, however, a relatively large deviation from the experimental data occurs close to the condenser end. Considering the complexities of the flow and heat transfer in the condenser section, Eqs. (33) and (34) are believed to be valid analytical solutions which can predict well, the temperature distributions along the heat pipe length.

6. Conclusions

Based on the analytical and experimental investigations presented in this paper, the following conclusions may be made:

1. The radially rotating miniature high-temperature heat pipe has a simple structure, low manufacturing cost, very high effective thermal conductance and large heat transfer capability. At the same time, the heat pipe can withstand strong vibrations and work in a high-temperature environment. Therefore, the turbine engine component cooling incorporating radially rotating miniature high-temperature heat pipes is a feasible and effective cooling method.
2. The non-condensable gases in the heat pipe have an adverse effect on the heat pipe performance. It results in a large temperature gradient near the condenser end and reduces the effective thermal conductance and heat transfer capability of the heat pipe.
3. Eqs. (33) and (34) predict reasonably well the temperature distributions along the heat pipe length and are a useful analytical tool for heat pipe design and performance analysis.

Acknowledgements

The authors would like to thank the Air Force Office of Scientific Research for the financial support and Dr. James McMichael of AFOSR for his interest in this research project.

References

[1] A. Faghri, Heat Pipe Science and Technology, Taylor and Francis, Washington DC, 1995.
[2] Y. Cao, Cao, Rotating micro/miniature heat pipes for turbine blade cooling applications, in: AFOSR Contractor and Grantee Meeting on Turbulence and Internal Flows, Atlanta, 1996.
[3] D.A. Dunn, P.D. Reay, Heat Pipe, Pergamon Press, Oxford, New York, 1982.
[4] S.W. Chi, Heat Pipe Theory and Practice: A Sourcebook, Hemisphere Publishing, New York, 1975.
[5] Y. Cao, W.S. Chang, Analyses of heat transfer limitations of radially rotating heat pipe for turbomachinery applications, in: AIAA Proceedings of the 32nd Thermophysics Conference, Atlanta, 1997.
[6] C. Harley, A. Faghri, Two-dimensional rotating heat pipe analysis, ASME Journal of Heat Transfer 117 (1) (1995) 418–426.
[7] P. Marto, Performance characteristics of rotating wickless heat pipes, in: Proceedings of the 2nd Int. Heat Pipe Conference, Bologna, 1976, pp. 281–291.
[8] T. Daniels, F. Al-Jumaily, Investigations of the factors affecting the performance of a rotating heat pipe, Int. Journal of Heat and Mass Transfer 18 (1975) 961–973.
[9] V.H. Gray, The rotating heat pipe — a wickless, hollow shaft for transferring heat fluxes, in: Proceedings of ASME/AIChE Heat Transfer Conference, Minneapolis, 1969, pp. 1–5.
[10] Y. Cao, J. Ling, W.S. Chang, Analyses of liquid and vapor flows in a miniature radially rotating heat pipe for turbine blade cooling applications, in: Proceedings of the 11th International Heat and Mass Transfer Conference, South Korea, 1998.
[11] J. Ling, Y. Cao, W.S. Chang, Analysis of radially rotating high-temperature heat pipes for turbomachinery application, ASME Journal of Engineering for Gas Turbines and Power 121 (2) (1999) 306–312.
[12] B.D. Marcus, Theory and design of variable conductance heat pipes: control techniques, 2nd report by TRW Inc. to NASA, 1971.
[13] J. Ling, Y. Cao, Experimental investigation of high-temperature radially rotating miniature heat pipes, ASME Journal of Heat Transfer, submitted for publication.